Green Chemistry

PAPER

View Article Online
View Journal | View Issue

Cite this: *Green Chem.*, 2026, **28**, 7836

Triacetic acid lactone conversion to methylene-δ-caprolactone: a renewable monomer for bio-based circular polymer synthesis

Camilo A. Ortega-Vega, †[a] Bowei Liu, †[b] Francesca D. Eckstrom,[c] Eswara Rao Chokkapu, [c] Eugene Y.-X. Chen, [c] Yuriy Román-Leshkov *[b] and Yomaira J. Pagán-Torres *[a]

Received 24th February 2026,
Accepted 21st April 2026

DOI: 10.1039/d6gc01148a

rsc.li/greenchem

To enable a circular and sustainable plastics economy, polymers must be derived from renewable carbon feedstocks and designed for chemical recyclability. Here, we report a multistep catalytic strategy for converting triacetic acid lactone (TAL), a biomass-derived platform chemical, into poly(α-methylene-δ-caprolactone) (PMCL), a more sustainable (bio-based and chemically recyclable) analogue of poly(methyl methacrylate) (PMMA). The process proceeds *via* the (i) quantitative hydrogenation of TAL to 4-hydroxy-6-methyltetrahydro-2-pyrone (HMTHP) catalyzed by Ru/C, (ii) HMTHP conversion to δ-caprolactone (dCL) over Pt/TiO_2 with 88% yield, (iii) Cs_2O/SiO_2 catalyzed vapor-phase aldol condensation of dCL with formaldehyde to methylene-δ-caprolactone (MCL) at 92% yield, and (iv) vinyl addition polymerization of MCL to PMCL. The resulting PMCL exhibits performance and recyclability advantages over its fossil-based linear analogue, PMMA. Overall, this work demonstrates the integration of selective catalytic biomass transformations with polymer synthesis to access recyclable vinyl polymers from a bio-based platform molecule.

Green foundation

1. This work advances green chemistry by converting glucose-derived triacetic acid lactone to a chemically recyclable polymer that matches or exceeds PMMA performance, enabling a renewable and more sustainable pathway to acrylic-like materials. By leveraging heterogeneous catalysis across the entire monomer synthesis route, the work demonstrates efficiency-driven process design for bio-based, circular acrylic analogues.
2. Each heterogeneous catalytic step was optimized for high performance, achieving a quantitative yield to HMTHP, 88% yield to dCL, and 92% yield to MCL. The bio-based polymer shows a higher glass transition temperature than PMMA and can be cleanly depolymerized to virgin monomer at 220 °C, demonstrating true chemical recyclability.
3. Future research will include technoeconomic analysis to assess economic viability and identify impactful process improvement. Additionally, optimizing monomer recovery beyond 74% will be a key goal to further strengthen circularity and sustainability.

Introduction

The widespread adoption of plastics derives from their durability, chemical stability, and low cost, which have enabled their use across healthcare, food security, and transportation.[1,2] However, the prevailing linear "take, make, dispose" model has precipitated an escalating environmental crisis, characterized by the accumulation of non-biodegradable waste and sustained reliance on fossil-carbon feedstocks.[3] Addressing this crisis requires a dual strategy: transitioning from fossil-based feedstocks to renewable biomass and re-engineering polymers for inherent circularity. While mechanical recycling suffers from cumulative polymer degradation, chemical recycling can recover monomers with virgin-level performance.[2] However, the high thermodynamic stability of commodity polymers, such as polyolefins and acrylates, typically necessitates energy-intensive conditions for chemical depolymerization, resulting in poor monomer selectivity. Bio-based monomers derived from oxygen-rich biogenic feedstocks, particularly lactones, enable polymers that retain the stability required for commodity applications while allowing selective closed-loop depolymerization under mild conditions.[4,5]

[a]*Department of Chemical Engineering, University of Puerto Rico-Mayaguez, Mayaguez, Puerto Rico, 00680, USA. E-mail: yomairaj.pagan@upr.edu*
[b]*Department of Chemical Engineering, Massachusetts Institute of Technology, Cambridge, Massachusetts, 02139, USA. E-mail: yroman@mit.edu*
[c]*Department of Chemistry, Colorado State University, Fort Collins, Colorado, 80523, USA*
† These authors contributed equally to this work.

Among commodity polymers, polymethyl methacrylate (PMMA) is therefore a priority target for lactone-based substitution due to its large market volume and associated lifecycle environmental burden.

PMMA is a transparent thermoplastic widely used as a substitute for inorganic glass due to its high impact resistance, high light transmittance, weather endurance, and dimensional stability.[6] It is employed in automobile lighting, conductive and optical devices, electronic displays, architectural panels, and biomedical applications.[7–9] The PMMA market reached approximately $1.2 billion in the United States and $4 billion globally in 2022, and is projected to expand at a compound annual growth rate of 5.4% by 2030.[5,10,11] Despite its versatility, conventional PMMA is derived from fossil-based methyl methacrylate (MMA), contributing to greenhouse emissions, estimated at around 3.8 million metric tons CO_2 per year.[5,12] Mechanical recycling of PMMA remains limited, accounting for less than 10%, due to polymer degradation during repeated processing.[10,13] Chemical recycling can recover monomers but typically requires depolymerization temperatures above 450 °C, which limits economic and environmental viability.[14,15]

To address these sustainability challenges, recent efforts have focused on developing bio-based monomers and PMMA analogues that combine renewable feedstocks with chemical recyclability. Diverse synthetic pathways have been explored to produce bio-derived acrylates and methacrylates from renewable organic acids and polyols.[16,17] For instance, the selective decarboxylation of itaconic acid and citric acid to methacrylic acid and its subsequent esterification with methanol has emerged as a prominent route to bio-based methyl methacrylate (MMA).[18–20] Polymers that have recently emerged as promising PMMA analogues include poly(α-methylene-γ-valerolactone) (PMGVL), poly(α-methyl-δ-valerolactone) (PMVL), and poly(α-methylene-δ-decalactone) (PMDL).[2,5,21] These polymers feature lactone-containing structures that enable selective depolymerization to their respective monomers under mild conditions, making them viable alternatives to fossil-derived PMMA. However, techno-economic analysis (TEA) indicates that the economic competitiveness of PMVL is primarily limited by the high cost of its δ-valerolactone (DVL) precursor, where approximately 77% of the PMVL production cost arises from lactone synthesis and its subsequent homogeneous aldol condensation to MVL.[5] A critical driver of this cost is the reliance on expensive diol feedstock, such as 1,5-pentanediol (PDO), which accounts for roughly 30% of the annual operating expenses ($1.92 per kg).[5] Furthermore, current synthetic routes rely on homogeneous catalysts and stoichiometric bases (*e.g.*, NaH), increasing separation requirements and waste generation, which limits scalability.[5,21] Consequently, existing bio-based PMMA substitutes fail to offer a decisive cost and environmental advantage over conventional fossil-derived PMMA, motivating alternative feedstock and catalytic strategies.

Bio-derived platform molecules that are low-cost and capable of modular transformation *via* heterogeneous catalysis are particularly desirable for establishing a circular polymer economy. Triacetic acid lactone (TAL) is a bio-privileged molecule known for its versatility in producing commercially valuable chemical intermediates.[22] TAL is a polyketide compound produced from glucose through engineered microbial fermentation using strains of *Saccharomyces cerevisiae*, *Escherichia coli*, or *Yarrowia lipolytica*.[23–25] Recent advances report TAL yields of 0.05 g g^{-1} glucose with titers of 9.9 g L^{-1} in antibiotic-free fed batch fermentation using engineered *Rhodotorula toruloides*, while techno-economic benchmarks for sugarcane-based production estimate a baseline minimum product selling price of approximately $4.60 per kg.[26,27] Process integration and biorefinery optimization are projected to reduce this value to $2.26 per kg, making bio-based TAL cost-competitive with fossil-derived precursors.[22,27] TAL is structurally rich in reactive functionalities, making it a highly versatile platform molecule for further transformation into high-value products such as sorbic acid, potassium sorbate, and δ-lactams.[26,28,29] Notably, TAL also serves as an entry point to sustainable materials, including highly recyclable polydiketoenamine plastics and PMMA analogues, offering a scalable, low-carbon alternative to traditional petroleum-based synthetic routes.[30]

In this work, we report a catalytic strategy for the conversion of TAL to methylene-δ-caprolactone (MCL) and its subsequent polymerization to poly(α-methylene-δ-caprolactone) (PMCL) (Scheme 1), a PMMA analogue with higher temperature resistivity and demonstrated chemical recyclability (*vide infra*). The pathway achieves high selectivity at each transformation step and avoids the use of homogeneous catalysts or stoichiometric bases. TAL undergoes (i) hydrogenation to 4-hydroxy-6-methyltetrahydro-2-pyrone (HMTHP), (ii) dehydration and hydrogenation of HMTHP to δ-caprolactone (dCL), (iii) aldol condensation of dCL with formaldehyde to MCL, and (iv) vinyl addition polymerization of MCL to PMCL. This sequence integrates biomass-derived feedstock upgrading with monomer synthesis and polymerization using catalytic steps compatible with scalable processing.

Experimental methods

Materials

All commercial chemicals were used as received. Triacetic acid lactone (Sigma-Aldrich, 98%), 5,6-dihydro-6-methyl-2*H*-pyran-2-one (Enamine, 97%), δ-caprolactone (Sigma-Aldrich, 98%), tetrahydrofuran (THF with BHT, Sigma-Aldrich, 99%), dioxane (Sigma-Aldrich, 98%), acetylacetone (Sigma-Aldrich, 99%), 4-hydroxy-2-pentanone (Enamine, 95%), formaldehyde (37 wt% formaldehyde in water, stabilized with methanol, Thermo Scientific), *trans*-3-hexenoic acid (Sigma-Aldrich, >97%), γ-caprolactone (Sigma-Aldrich, >98%), methyl-*trans*-3-hexenoate (Sigma-Aldrich, >97%), hexanoic acid (Sigma-Aldrich, 99%), trioxane (Sigma-Aldrich, >99%), sulfuric acid (Fisher, 97%), zirconium dinitrate oxide hydrate (Thermo-Scientific, 99.9%), ammonium hydroxide solution (Fisher, 27–30%), palladium(II) nitrate dihydrate (Sigma-Aldrich), platinum(IV) chloride (Sigma-Aldrich), calcium acetate monohy-

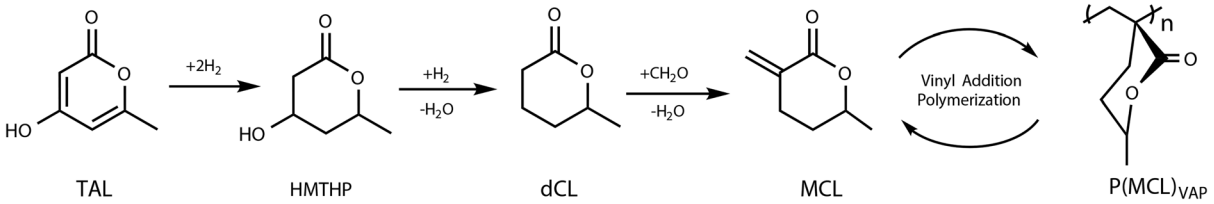

Scheme 1 Multistep catalytic strategy for PMCL synthesis from TAL.

drate (Sigma-Aldrich, >99%), barium acetate (Sigma-Aldrich, >99%), and cesium acetate (Sigma-Aldrich, >99%). Commercial catalysts and supports used include 5 wt% Ru/C (Sigma-Aldrich), 5 wt% Pd/C (Sigma-Aldrich), 5 wt% Ru/Al_2O_3 (Sigma-Aldrich), 5 wt% Pd/Al_2O_3 (Sigma-Aldrich), SIRAL 40 (Sasol), SIRAL 70 (Sasol), titanium(IV) oxide P25 (Sigma-Aldrich), cerium oxide support (CeO_2, Daiichi Kigenso), gamma-alumina (γ-Al_2O_3, Strem Chemicals), silicon(IV) oxide amorphous nanopowder (SiO_2, Alfa Aesar). The ZrO_2 support was synthesized by coprecipitation using ammonia as a precipitant. Typically, zirconium dinitrate oxide hydrate (5.015 g) was diluted in 100 mL of DI water. Next, a 28% ammonium hydroxide solution was added dropwise into the zirconium solution while stirred at room temperature until the pH = 7. The resulting slurry was stirred at room temperature for 24 h, during which the slurry reached a pH = 9. The precipitate was recovered by centrifugation (5000 rpm for 5 min) and washed multiple times with DI water until the pH of the solution was neutral. The recovered powder was dried overnight at 120 °C. Finally, the material was calcined in a muffle furnace under air at 500 °C with a ramp rate of 2 °C min^{-1} and a hold time of 2 h.

Air and moisture-sensitive reactions were conducted in oven- or flame-dried glassware on a dual manifold N_2/vacuum Schlenk line or inside an N_2-filled glovebox. HPLC-grade toluene was first sparged extensively with nitrogen during filling 20 L solvent reservoirs and then dried by passage through activated alumina. Toluene was additionally stirred over CaH_2 for 12 hours followed by vacuum distillation and filtration. The solvent was stored in an N_2-atmosphere glovebox over NaK and filtered through a 0.22 μm nylon filter prior to use. The following reagents were used as received: La[N$(SiMe_3)_2]_3$ (Sigma-Aldrich). Azobisisobutyronitrile (AIBN) was purchased from Sigma Aldrich, dried under vacuum at 25 °C for 2 days, transferred to an N_2-atmosphere glovebox, and stored at −30 °C. Benzyl alcohol (BnOH) initiator, purchased from TCI, was stirred over CaH_2 for 12 h under N_2 then vacuum distilled at 100 °C under 50 mTorr. It was then transferred to an N_2-atmosphere glovebox, filtered through a 0.22 μm filter and stored at −30 °C in a brown bottle.

Prior to polymerization, MCL was transferred to a Schlenk flask and put under vacuum at 25 °C for 30 minutes, then transferred to an N_2-atmosphere glovebox and stored in a brown bottle at −30 °C over 4 Å molecular sieves. The monomer was then used without further purification. For comparison studies, MCL was also synthesized according to the procedure detailed below. The synthesized MCL was dried by stirring over CaH_2 for 12 h under N_2 prior to vacuum distillation at 50 °C under 50 mTorr. The purified monomer was brought into an N_2 atmosphere glovebox, filtered through a 0.22 μm filter, and stored at −30 °C in a brown bottle.

HMTHP synthesis

Since HMTHP is not commercially available, the compound was synthesized and purified from the hydrogenation of TAL using a 5 wt% Ru/C (Sigma-Aldrich). In a typical experiment, 500 mg of TAL was dissolved in 24 g of THF and 125 mg of 5 wt% Ru/C were added in a 50 mL Parr reactor equipped with a magnetic stir bar. The reactor was sealed and purged three times with N_2 and then three times with H_2 and subsequently pressurized to 35 bar H_2. The reaction was carried out at 60 °C for 2 h at a stirring speed of 740 rpm. After completion, the reactor was cooled to room temperature by directing a continuous air stream over the external surface. The catalyst was removed from the product mixture through a 0.22 μm PTFE filter, and HMTHP was then isolated from the product mixture through solvent evaporation. The isolated HMTHP (97.2% pure as measured by ^{1}H NMR) was used to prepare calibration standards for GC analysis. A detailed description of NMR analysis results can be found in the SI (Fig. S1–S3).

Catalyst synthesis

Monometallic catalysts Pt/TiO_2, Pt/CeO_2, Pt/ZrO_2, Pt/SiO_2 and Pt/Al_2O_3 (containing 1 wt% Pt) and Pd/SIRAL (5 wt% Pd) were prepared by incipient wetness impregnation. For Pt-supported catalyst, an aqueous solution of $PtCl_4$ was deposited on TiO_2 (P25), ZrO_2, γ-Al_2O_3, CeO_2 and SiO_2. For Pd-supported catalyst, aqueous solutions of $Pd(NO_3)_2{\cdot}2H_2O$ were deposited on SIRAL 40 and SIRAL 70. Catalysts were then dried overnight at 120 °C and calcined in air at 500 °C for 3 h.

For aldol condensation reactions, supported catalysts were synthesized *via* incipient wetness impregnation. Fumed silica served as the support and was pre-calcined at 550 °C in air (ramp rate: 3 °C min^{-1}; hold: 4 h; air flow: 120 mL min^{-1}). Calcium acetate monohydrate, barium acetate, or cesium acetate was dissolved in deionized water to achieve the desired metal loading. The impregnation volume was fixed at 4.4 mL of aqueous solution per gram of SiO_2. After impregnation, the samples were dried at 80 °C for 16 h and calcined at 550 °C under identical conditions to the support pre-treatment. The

calcined material was crushed and sieved to retain particles in the 250–500 μm range for catalytic testing.

MCL synthesis

To compare the polymerization results with MCL produced by the process developed in this work, a batch of MCL was synthesized using an organic synthesis route. A suspension of NaH (60 wt% dispersion in mineral oil, 5.8 g, 0.24 mol, 2.75 equiv.) in anhydrous THF (60 mL) was cooled to 0 °C. A solution of δ-hexalactone (10.0 g, 88 mmol, 1.00 equiv.) and diethyl oxalate (13.0 g, 88 mmol, 1.01 equiv.) in THF was added dropwise to the NaH suspension at 0 °C. After the addition was complete, the reaction mixture was stirred at 0 °C for 10–15 min. Absolute ethanol (3.4 g, 74 mmol, 0.85 equiv.) was then added dropwise at 0 °C over 15 min (gas evolution observed). The reaction mixture was allowed to warm to room temperature and stirred for 3 h. The reaction mixture was cooled again to 0 °C, then saturated aqueous K_2CO_3 solution (49 g, 0.35 mol, ~4 equiv.) and formalin (37 wt% aqueous solution, 98 g, 3.3 mol, 37.1 equiv.) were added sequentially. The biphasic mixture was stirred at 0 °C for 30 min, then diethyl ether (100 mL) was added, and the mixture was stirred for an additional 30 min. The organic layer was separated, and the aqueous layer was extracted with diethyl ether. The combined organic layers (THF/Et_2O) were washed with brine, dried over Na_2SO_4, filtered, and concentrated under reduced pressure. The crude product was purified by column chromatography (hexanes/EtOAc = 5 : 1) to afford the product as a pale-yellow oil (83% yield). ^{1}H NMR (400 MHz, $CDCl_3$, ppm) δ 6.40 (s, 1H), 5.55 (s, 1H), 4.47–4.48 (m, 1H), 2.53–2.71(m, 2H), 1.94–1.98 (m, 1H), 1.64–1.67 (m, 1H), 1.38–1.39 (d, 3H).

Characterization

CO_2 uptake measurements were conducted using thermogravimetric analysis (TGA) on a TA Instruments Q500 thermogravimetric analyzer. Samples were pretreated under flowing N_2 (50 mL min^{-1}) at 450 °C (ramp rate: 3 °C min^{-1}; hold: 4 h), then cooled, and equilibrated at 50 °C. CO_2 adsorption was carried out by exposing the samples to a CO_2/N_2 mixture (45 mL min^{-1} CO_2 in 5 mL min^{-1} N_2) for 1 h, followed by purging with N_2 (50 mL min^{-1}) for 1 h. Desorption was monitored by ramping the temperature stepwise to 150 °C, 250 °C, 350 °C, and 450 °C (3 °C min^{-1} under N_2 flow), holding for 1 h at each step. Total and temperature-resolved CO_2 uptake was quantified relative to the final sample mass at 450 °C under N_2.

Nitrogen physisorption isotherms were measured on a Micromeritics 3Flex instrument at 77 K. Prior to analysis, samples were outgassed under vacuum (<5 μmHg) for 4 h at 300 °C. Surface areas were estimated using Brunauer–Emmett–Teller (BET) analysis. Carbon monoxide chemisorption of Pt-based catalysts was conducted in a Micromeritics AutoChem II 2920 unit equipped with a thermal conductivity detector. The catalyst sample (0.1 g) was loaded in a U-shaped quartz reactor between two quartz wool plugs and pretreated in hydrogen (50 mL min^{-1}) at 450 °C (ramp rate: 3 °C min^{-1}; hold: 4 h) before purging and cooling to 45 °C in He (50 mL min^{-1}). Then pulse doses of CO (1% CO/He) were injected onto the sample until saturated. The combined CO uptake n_{CO} was taken as the number of accessible Pt sites and used to calculate site density, where m_{cat} is the mass of catalyst:

$$\varphi = \frac{n_{CO}}{m_{cat}}$$

Powder X-ray diffraction (XRD) patterns were acquired using a Bruker D8 diffractometer equipped with a Cu Kα radiation source. Data were collected over a 2θ range of 10–90° at a scan rate of 0.05° s^{-1}. Scanning transmission electron microscopy (STEM) was performed using a probe-corrected Thermo Fisher Scientific Themis Z G3 microscope operated at 200 kV. Images were collected using a 19 mrad probe convergence angle and detector collection angles of 70–200 mrad for high-angle annular dark field (HAADF, *Z*-contrast) imaging. Energy dispersive spectroscopy (EDS) was performed using a dual silicon drift detector (Thermo Fisher Dual-X) with an energy resolution of 129 eV at Mn Kα.

For hydrogenation, dehydration, and aldol condensation, NMR spectra were collected on a Bruker Avance Neo 500 MHz spectrometer (500 MHz, ^{1}H; 125 MHz, ^{13}C). For polymerization, NMR spectra were collected on a Bruker AV-III 400 MHz spectrometer (400 MHz, ^{1}H; 100 MHz, ^{13}C). Chemical shifts for ^{1}H and ^{13}C spectra were referenced to internal solvent resonance 7.26 (chloroform) and are reported as parts per million relative to $SiMe_4$. Monomer conversion and copolymer composition were calculated based on relative integrations between monomer and polymer ^{1}H NMR signals.

Polymer absolute weight-average molecular weight (M_w), number-average molecular weight (M_n), and molecular weight distributions ($Đ = M_w/M_n$) were measured *via* size exclusion chromatography (SEC). The SEC instrument consisted of an Agilent HPLC system equipped with one guard column and two PLgel 5 μm mixed-C gel permeation columns, coupled with a Wyatt DAWN HELEOS II multi (18)-angle light scattering detector and a Wyatt Optilab TrEX dRI detector. Measurements were taken at 40 °C using chloroform as the eluent at a flow rate of 1.0 mL min^{-1}. Samples were analyzed with Wyatt ASTRA 8.2.0 molecular weight characterization software, assuming 100% mass recovery, which calculated a dn/dc of 0.0876 internally, based on sample concentration of 2.63 mg mL^{-1}.

All thermal analysis was performed on polymer samples that were dried at 60 °C for 12 h under 40 mTorr. Differential Scanning Calorimetry (DSC) was performed on a TA 2500 Modulated Differential Scanning Calorimeter and data was analyzed with the TRIOS software package. DSC Plots show the glass transition temperature (T_g) obtained from a second heating scan. Each cycle was performed at a rate of 10 °C min^{-1}. Decomposition temperatures ($T_{d5\%}$, defined by the temperature of 5% weight loss) of the polymers were measured with TGA by heating from ambient temperature to 700 °C at 10 °C min^{-1} under N_2 on a TGA-55 (TA Instruments) with an evolved gas analysis furnace (TA instruments). TGA data were

processed with the TRIOS software package. Values of $T_{d5\%}$ were obtained from wt% *vs.* temperature (°C) plots.

Transmission measurement for polymer optical properties was performed on a Shimadzu UV-3600i UV-vis/NIR spectrophotometer, equipped with MPC-603A integrating sphere accessory, using the standard wide-open sampling port. The samples were scanned from 1000 nm to 200 nm at a rate of 1 nm s^{-1} with a data interval of 1 nm. The detector crossover from InGaAs to PMT was set at 860 nm.

Reactivity test

Hydrogenation and dehydration reactions were performed in a 50 mL high-pressure batch reactor (Parr Instrument, 4792). For each reaction, the desired amount of reactant (TAL or HMTHP), THF, catalyst, and magnetic stir bar were added to the batch reactor. After sealing the reactor, it was purged three times with N_2 and then three times with H_2 to ensure complete removal of residual air. The reactor was then pressurized with H_2 (35 bar), followed by heating to the desired reaction temperature (60–160 °C), and stirring at 740 rpm. Upon completion of the reaction time, the reactor was cooled by directing a continuous flow of air over its external surface. After the reaction, the catalyst was filtered, and the liquid products were quantified by high-performance liquid chromatography (HPLC, Waters Alliance e2695) and gas chromatography (GC, Agilent 7890B). HPLC analysis was conducted for TAL quantification. The Waters HPLC was equipped with a Bio-Rad Aminex HPX-87H column (300 mm × 7.8 mm) and Waters 2414 refractive index detector, operating at 30 °C and 0.005 M H_2SO_4 solution at 0.55 mL min^{-1}. The Agilent GC was equipped with a SHRXI-5MS capillary column (Shimadzu, 15 m × 0.53 mm ID × 0.25 μm) and a flame ionization detector (FID, Agilent). GC analysis was used for the identification and quantification of HMTHP, 5,6-dihydro-4-hydroxy-6-methyl-2*H*-pyran-2-one (DHMP), parasorbic acid (PSA), acetylacetone, hexanoic acid, 4-hydroxy-2-pentanone, and dCL.

Aldol condensation of dCL and formaldehyde (37 wt% formaldehyde in water, stabilized with methanol) was conducted over SiO_2-supported base catalysts (sieved to 250–500 μm) in a downflow packed bed reactor. Gas flows were controlled by mass flow controllers (Brooks GF40), and liquids were delivered *via* syringe pumps (Harvard 11 Elite) through capillary tubing. For catalyst masses below 0.5 g, the catalyst was diluted with silicon carbide (350 μm) to a total bed mass of 0.5 g and loaded into a $\frac{1}{4}''$ 316 stainless steel tube. For catalyst masses above 0.5 g, undiluted samples were packed directly into a $\frac{3}{8}''$ 316 stainless steel tube. Quartz wool plugs were used to secure the bed, and ~1.0 g of borosilicate glass beads was added atop the bed to promote premixing of vapors.

The reactor was heated in a tube furnace (ATS system), with temperature controlled by a Digi-Sense controller (Cole-Parmer R/S 68900-11) using a K-type thermocouple positioned just below the bed. Reactor effluent was monitored online using a gas chromatograph (Agilent 8890) equipped with an HP-5 ms column and FID detector. Liquid products were collected in a toluene bubbler and identified by GC-MS (Agilent 7890 with 5975C MSD). All transfer lines were heat-traced at >300 °C to prevent condensation. Prior to experiments, the catalyst bed was calcined with air (50 mL min^{-1}, 500 °C, 3 °C min^{-1}, 4 h) before being purged with nitrogen. For reactions using dCL and formalin, a premixed feed was vaporized and merged with the nitrogen carrier gas stream in a stainless-steel tee heated to 240 °C. For trioxane-based feeds (37 wt% in methanol or THF), the trioxane solution was vaporized at 110 °C, carried by nitrogen flow through a 400 °C decomposition zone, and then joined with the dCL vapor stream upstream of the reactor. Catalysts deactivate rapidly upon exposure to the reactant stream. For consistent comparison, all reported rates correspond to steady state, defined as <5% variation in product formation rates over 2 h, reached after at least 20 h on stream. Contact time was varied by adjusting the total flow rate at constant reactant concentrations. The catalyst bed was regenerated by repeating the calcination procedure described above. Contact time in the packed bed reactor was calculated as:

$$\tau = \frac{m_{cat}}{\dot{m}_{tot}}$$

where m_{cat} is the total mass of the catalyst in the reactor, and $\dot{m}_{tot}$ is the total mass flow rate of all feed components entering the reactor.

The conversion (x) of reactant (j) and selectivity (S) to product (i) were calculated as:

$$X = \frac{n_{0(j)} - n_{f(j)}}{n_{0(j)}} \times 100$$

$$S_i = \frac{n_{f(i)}}{n_{0(j)} - n_{f(j)}} \times 100$$

where n_0 and n_f refers to initial and final moles for hydrogenation and dehydration, or initial and final molar flow rates for aldol condensation. Any carbon deficit in the aldol condensation mass balance was assigned to lost carbon, with selectivity defined as:

$$S_{\text{lost carbon}} = 1 - \sum_i S_i$$

Polymerization procedures

PMCL (radical). In an N_2-supplied atmosphere glovebox, 0.0006 g of AIBN were added to 0.539 g MCL solubilized in 2 mL toluene in a pressure vial ([MCL] : [I] = 1000 : 1). The reaction vial was transferred to an oil bath and brought to 80 °C while stirring. After 24 h, the reaction was quenched by exposure to air. An aliquot of the quenched mixture was taken for analysis with ^{1}H NMR, confirming 43–44% conversion of MCL to PMCL. The reaction mixture was precipitated into cold ethyl acetate. The precipitate was resolubilized in $CHCl_3$, precipitated twice more in ethyl acetate and once in diethyl ether. The purified polymer was then dried at 60 °C in a vacuum oven over 12 h to reveal 0.119–0.173 g of pure polymer (22–32% yield).

PMCL (coordination-addition). In an N_2-supplied atmosphere glovebox, 0.50 g of MCL and 1.98 mL toluene were added to a 20 mL scintillation vial equipped with a PTFE-

coated magnetic stir bar. Separately, 0.002 g of $La[N(SiMe_3)_2]_3$ was dissolved in a minimal amount of toluene and added to 3 equivalents (0.0013 g) of BnOH and allowed to stir for 5–10 min to form the desired lanthanum alkoxide initiator ($[MCL]:[[La(OBn)_3]_x] = 1000:1$). The mixture was then transferred to the MCL solution and allowed to react at 25 °C. After 6 h, the reaction was quenched with a few drops of acidified MeOH and an aliquot was taken for analysis with ^1H NMR, confirming 99% conversion to PMCL. The reaction mixture was diluted with $CHCl_3$ and precipitated into cold ethyl acetate. The precipitate was resolubilized in $CHCl_3$, precipitated twice more in ethyl acetate and once in diethyl ether. The purified polymer was then dried at 60 °C in a vacuum oven over 12 h to reveal 0.361 g of pure polymer (71% yield).

Depolymerization procedures

PMCL (0.2 g) was placed in a flame-dried reaction flask and fitted to a short-path distillation apparatus equipped with a receiving flask. The system was connected to a high-vacuum line, evacuated to 50 mTorr, and the receiving flask was cooled in a dry ice/acetonitrile bath. With the system under continuous vacuum (50 mTorr), the reaction flask was heated to 220 °C and maintained at this temperature for 11 h. During this period, MCL distilled from the reaction flask into the receiving flask. After reaction completion, the apparatus was allowed to come to room temperature, and the monomer was collected as a colorless liquid and weighed to calculate the yield (0.148 g, 73.9%). An additional 0.024 g of oligomeric PMCL collected from the reaction flask accounted for another 12% of the mass balance, and the remaining 14.1% uncollected mass was attributed to transfer loss.

Results and discussion

TAL hydrogenation to HMTHP

Heterogeneous catalysts based on supported Pd, Pt, and Ru have been reported for TAL hydrogenation to HMTHP.[28,31] Accordingly, we screened a series of supported Ru, Pd, and Pt catalysts for this reaction (Table 1), aiming to maximize HMTHP selectivity at complete TAL conversion while suppressing ring-opening and decarboxylation byproducts such as acetylacetone, 3-penten-2-one, and 4-hydroxy-2-pentanone (Scheme 2).

Over 5 wt% Pd/Al_2O_3 and 5 wt% Ru/Al_2O_3, TAL was converted to HMTHP with 83% and 88% selectivity, respectively, with the balance comprising the decarboxylation products acetylacetone and 4-hydroxy-2-pentanone (Table 1, entries 1 and 2). Replacing Al_2O_3 with the acidic SIRAL support decreased HMTHP selectivity while increasing selectivity to acetylacetone and 4-hydroxy-2-pentanone (Table 1, entries 3 and 4). The Brønsted and Lewis acid sites on SIRAL promote hydrolysis, destabilizing the TAL and DHMP lactone rings, and facilitate decarboxylation through enolization and protonation pathways.[31–33]

TAL hydrogenation over 5 wt% Pd/C and 5 wt% Ru/C achieved 92% and 98.6% HMTHP selectivity, respectively, at complete conversion (Table 1, entries 5 and 6). Despite 5 wt% Pd/C resulting in high selectivity to HMTHP, trace amounts of 4-hydroxy-2-pentanone were still produced. Thus, 5 wt% Ru/C was identified as the optimal catalyst for quantitative TAL hydrogenation to HMTHP at 60 °C and 35 bar H_2.

HMTHP conversion to dCL

The catalytic activity and selectivity of Pt-supported catalysts in HMTHP conversion to dCL at 160 °C, 35 bar H_2, and 2 h of reaction time are reported in Table 2. The surface areas and metal dispersions for 1 wt% Pt-supported on various amphoteric metal oxide supports (TiO_2, Al_2O_3, CeO_2, ZrO_2) are summarized in Table S1. Among the Pt-based catalysts studied for HMTHP conversion, 1 wt% Pt/TiO_2 resulted in the highest activity for dCL formation (44% conversion of HMTHP, 88.7% selectivity) within 2 hours of reaction time despite its relatively low surface area (52 $m^2\ g^{-1}$) and Pt site density (10.2 μmol g_{cat}^{-1}) (Table S1 and Fig. S4). Upon increasing the reaction time to 8 hours, full conversion of HMTHP was obtained with a dCL selectivity of 87.5% (Table 2, entry 2). The other main product observed was hexanoic acid resulting from the subsequent ring-opening and hydrogenation of dCL to hexanoic acid. The performance observed for 1 wt% Pt/TiO_2 can be attributed to the bifunctional nature of the catalyst, where the support facilitates PSA formation through oxygen-vacancy sites and mild acidity, favoring the deoxygenation pathway, as

Table 1 TAL hydrogenation over different metal (Pd, Ru, Pt) supported catalysts[a]

			Selectivity (%)			
Entry	Catalysts	TAL conv. (%)	HMTHP	dCL	Acetylacetone	4-Hydroxy-2-pentanone
1	$Pd/\gamma\text{-}Al_2O_3$	100	83.7	4.2	6.3	4.8
2	$Ru/\gamma\text{-}Al_2O_3$	100	88.4	0.9	6.7	3.2
3	Pd/SIRAL 40	100	67.0	4.7	11.1	17.0
4	Pd/SIRAL 70	100	63.0	8.2	2.2	26.4
5	Pd/C	100	92.0	6.0	—	2.0
6	Ru/C	100	98.6	1.2	—	—
7	Pt/TiO_2	100	7.9	6.2	27.0	58.9

[a] Reaction conditions: TAL (3.9 mmol), THF (24 g), catalyst mass (125 mg), H_2 pressure (35 bar), reaction temperature (60 °C), reaction time (2 h), 740 rpm. Metal loadings for M/support (5 wt% M = Pd, Ru; 1 wt% Pt). Carbon balances for all reactions reported are >99%.

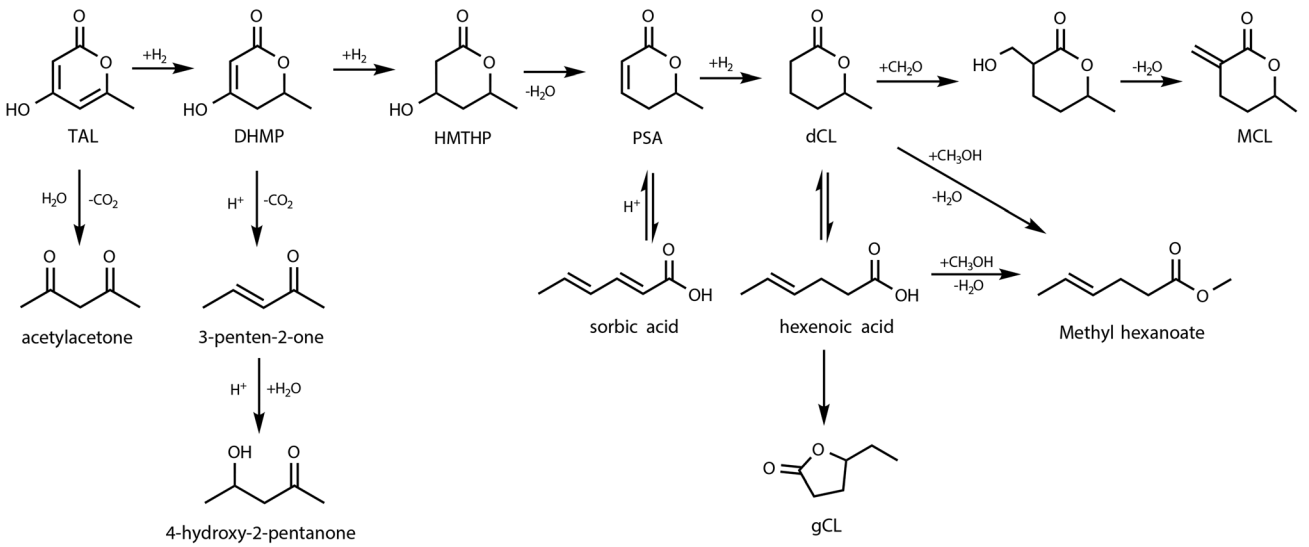

Scheme 2 Reaction pathways for TAL conversion to MCL including undesired decarboxylation, ring-opening, esterification and dehydration reactions.

Table 2 HMTHP conversion to dCL over Pt-supported catalysts[a]

Entry	Catalysts	Reaction time (h)	HMTHP Conv. (%)	Selectivity (%)		
				dCL	PSA	Hexanoic acid
1	Pt/TiO_2	2	44.4	88.7	1.7	6.8
2	Pt/TiO_2	8	100	87.5	0	7.4
3	Pt/CeO_2	2	32.1	77.2	5.4	12.1
4	Pt/ZrO_2	2	8.7	90.3	0	9.6
5	$Pt/\gamma\text{-}Al_2O_3$	2	18.4	90.4	0	9.1
6	Pt/SiO_2	2	0	0.0	0	0
7	TiO_2	2	16.5	0.0	100	0
8	TiO_2 [b]	2	13.1	0.0	100	0

[a] Reaction conditions: HMTHP (3.8 mmol), THF (22 g), catalyst (125 mg, 1 wt% Pt/support), H_2 pressure (35 bar), 160 °C, 740 rpm. [b] N_2 pressure (35 bar). Carbon balances for all reactions reported are >95%.

shown in Table 2, entries 7 and 8 for bare TiO_2, while Pt activates hydrogen for C=C bond saturation of PSA to dCL (Scheme 2).[34–37] When varying the support from TiO_2 to CeO_2, ZrO_2, and $\gamma\text{-}Al_2O_3$ for Pt-based catalysts, lower activities for dCL conversion at reaction times of 2 h are obtained of 32.1%, 8.7%, and 18.4% (Table 2, entries 3–5), respectively, despite these catalyst systems exhibit higher surface areas and Pt site density (Table S1, entries 2–4) compared to Pt/TiO_2. Notably, Pt/SiO_2 did not show catalytic activity (Table 2, entry 6), which can be explained by the inert nature of the SiO_2 support towards dehydration chemistries under the reaction conditions studied.

Aldol condensation of dCL and formaldehyde to MCL

Having successfully generated dCL from TAL, we next investigated its heterogeneous aldol condensation to MCL. Aldol condensation of analogous lactones such as γ-valerolactone (GVL) and DVL has been reported over BaO/SiO_2 and CaO/SiO_2 in continuous vapor-phase reactors, achieving >95% selectivity at ~40% conversion at 340 °C.[38] In the liquid phase, Cs_2O-supported β-zeolites are active at 280–310 °C in methyl-tetrahydrofuran.[2,39] However, the reactivity of dCL in aldol condensation is largely unexplored, and its condensation to MCL has not been previously reported. As a baseline, we selected silica-supported alkali and alkaline earth metal oxides (5 wt% CaO, BaO, and Cs_2O/SiO_2) for vapor-phase condensation. Note that under the water-rich conditions of the feed, these species are expected to convert to hydroxides. We nonetheless refer to them as metal oxides to reflect their pretreated state.

Textural and basicity properties of the catalysts are summarized in Table S2. All impregnated samples showed reduced surface area relative to the parent SiO_2, likely due to surface reorganization induced by interactions with strong bases during synthesis. Despite higher molar metal loading on CaO/SiO_2, qualitative CO_2 adsorption measurements indicate comparable surface basic site densities across the three catalysts, possibly reflecting weaker basic sites on CaO/SiO_2 that interact less strongly with CO_2. Cs_2O/SiO_2 exhibited the highest CO_2 uptake at elevated desorption temperatures, consistent with the stronger basic character of alkali metal oxides.[40] PXRD (Fig. S5) revealed no crystalline diffraction features beyond a broad amorphous silica feature near 2θ = 22°. STEM-EDS (Fig. S6) showed no discernible nanoparticles and uniform elemental distributions, indicating that the metal oxides are highly dispersed across the silica surface.

Selectivity and conversion data for the aldol condensation of dCL at 240 °C are summarized in Fig. 1a. All three catalysts exhibited significant ring-opening reactivity, an unexpected result given prior aldol condensation studies of GVL and

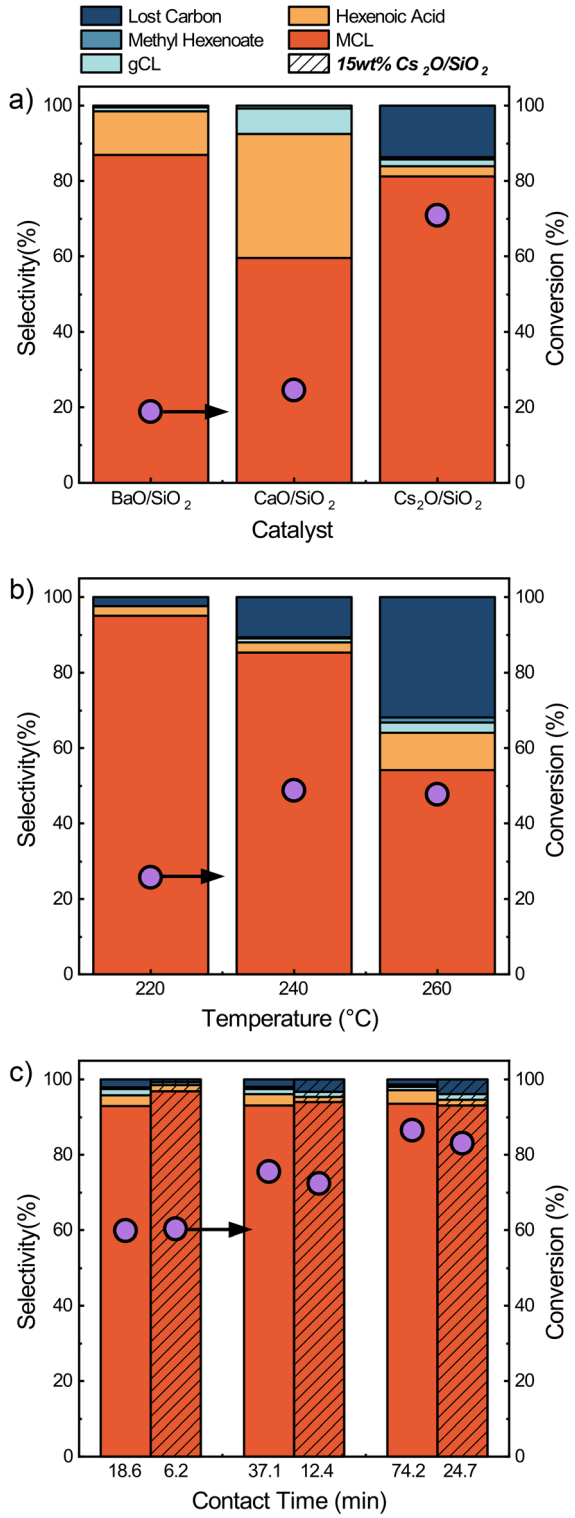

Fig. 1 Product distribution (bar chart) and dCL conversion (scatter) during aldol condensation reaction of dCL and formalin. Condition: 0.4 mol% dCL, 1.2 mol% formaldehyde, 1 bar, N_2 balanced. (a) Catalyst activity comparison at 240 °C with a fixed contact time of 9.3 min. (b) Effect of changing temperature on 5 wt% Cs_2O/SiO_2 catalyst with contact time of 4.6 min. (c) Influence of varying contact times at 220 °C for 5 wt% and 15 wt% Cs_2O/SiO_2 catalysts. Juxtaposed conditions represent experiments with the same amount of Cs loaded.

DVL.[2,38] As illustrated in Scheme 2, the proposed reaction network involves nucleophilic ring-opening of dCL by water or methanol in formalin, followed by dehydration to form hexenoic acid and methyl hexenoate over the basic catalyst surface. Formation of γ-caprolactone (gCL), observed across all catalysts, likely arises from acid-catalyzed ring closure of hexenoic acid and is consistent with prior reports over acidic metal oxide surfaces.[31]

Among the catalysts tested, Cs_2O/SiO_2 achieved the highest overall conversion of 71% while suppressing the selectivity of ring-opening side reactions to a combined 5%. In contrast, BaO/SiO_2 and CaO/SiO_2 gave markedly lower conversions (19% and 25%, respectively) and substantially higher ring-opening selectivities (13% and 40%, respectively), consistent with their weaker basic sites.[39] However, reaction over Cs_2O/SiO_2 exhibited substantial carbon loss with selectivity of 14%, primarily attributed to oligomerization, as evidenced by the presence of heavy species in the GC traces (Fig. S7). Similar carbon losses have been reported during DVL aldol condensation over strong bases at elevated temperatures.[2,38,39] These results suggest that the high basicity of Cs_2O/SiO_2 enhances aldol condensation activity while partially suppressing undesired ring-opening pathways. Thus, Cs_2O/SiO_2 was selected as the catalyst for further optimization.

To identify the optimal temperature for selective aldol condensation, a temperature study was conducted over 5 wt% Cs_2O/SiO_2 (Fig. 1b). Conversion of dCL increased from 220 °C to 240 °C, but MCL selectivity declined in favor of carbon loss, driven primarily by faster dimerization and coke formation at elevated temperatures. At 260 °C, substantial coking caused severe deactivation, reducing conversion to 48%, which is comparable to the 49% observed at 240 °C. These results indicate that an operating temperature of 220 °C is required to maintain high MCL selectivity (>95%).

A contact time study for the aldol condensation of dCL over 5 wt% Cs_2O/SiO_2 at 220 °C is shown in Fig. 1c (shorter contact times of 2.3–9.3 min are provided in Fig. S8a). Increasing contact time raised overall conversion while MCL selectivity remained largely unchanged. The apparent carbon loss at 220 °C was attributed primarily to measurement uncertainty rather than coking, as the carbon balance varied non-monotonically with contact time. At the longest contact time examined (74.2 min), conversion reached 87% with 92% MCL selectivity.

To increase the MCL production rate per unit catalyst mass, the cesium loading was tripled to 15 wt% *via* the same incipient wetness impregnation method. PXRD (Fig. S5a) and STEM imaging (Fig. S9) showed no crystalline diffraction features or observable particles, indicating that high dispersion was retained at this loading. Although qualitative, CO_2 uptake measurements (Table S2) confirmed an increase in accessible basic sites from 303 to 600 μmol g^{-1} with the higher cesium content. The 15 wt% Cs_2O/SiO_2 catalyst achieved comparable conversion and selectivity to the 5 wt% formulation at one third of the contact time (Fig. 1c), consistent with its greater density of active basic sites. At a contact time of 48 min, 15 wt% Cs_2O/SiO_2 reached 96% conversion and 95% selectivity (Fig. S8b), corresponding to a near-quantitative MCL yield. The MCL sample collected under these conditions was charac-

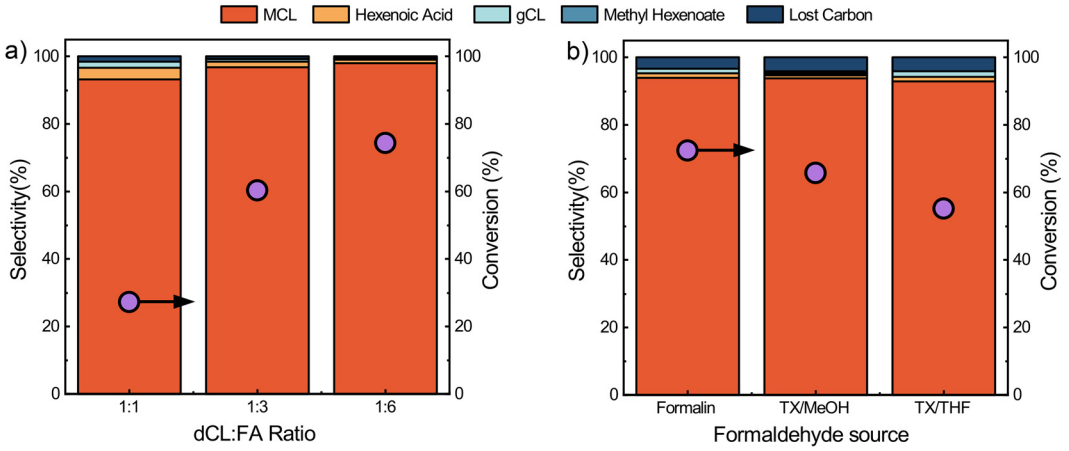

Fig. 2 Product distribution (bar chart) and dCL conversion (scatter plot) for the aldol condensation reaction over 15 wt% Cs_2O/SiO_2. (a) Effect of the formaldehyde-to-dCL molar ratio in the feed. Reaction conditions: contact time = 6.3 min; dCL = 0.4 mol%; 220 °C; 1 bar; N_2 balanced. (b) Effect of formaldehyde source on catalytic performance. Reaction conditions: contact time = 12.4 min; dCL = 0.4 mol%; formaldehyde = 1.2 mol%; 220 °C; 1 bar; N_2 balanced.

terized by ^1H and ^{13}C NMR (Fig. S10) and used for the polymerization step.

The effect of the formaldehyde-to-dCL molar ratio on aldol condensation over 15 wt% Cs_2O/SiO_2 is shown in Fig. 2a. Increasing the ratio to 6 : 1 improved conversion by approximately 15% while maintaining high MCL selectivity above 95%. In contrast, reducing the ratio to 1 : 1 decreased conversion by 33% and increased side product formation. A 3 : 1 ratio was therefore identified as a practical balance between feedstock economy and product yield.

To minimize ring-opening reactions associated with water and methanol in formalin, trioxane was tested as an alternative formaldehyde source. Above 300 °C, trioxane thermally decomposes to release three equivalents of formaldehyde per mole of trimer, providing a controlled feed without introducing species that facilitate ring opening.[39–41] However, when trioxane solutions in methanol or THF were used to replace formalin over 15 wt% Cs_2O/SiO_2, dCL conversion decreased substantially from 72% to 66% and 55% (Fig. 2b), likely due to incomplete decomposition of the precursor. Surprisingly, ring-opening selectivity remained comparable to that observed with formalin. We attribute this to water generated during dehydration of the aldol intermediates, which drives ring opening regardless of the formaldehyde source. Because water formation is inherent to MCL production, formalin was retained as the preferred reagent given its high reactivity, commercial availability, and minimal pretreatment requirements.

Catalyst reusability was demonstrated through multiple regeneration cycles (Fig. S11a). Conversion declined from 97% to 65% after 9 h on stream, and calcination in air at 500 °C for 4 h fully restored activity to 97% conversion. This deactivation-regeneration profile was reproducible over three consecutive cycles. Thermogravimetric analysis of spent 15 wt% Cs_2O/SiO_2 catalyst (Fig. S11b) revealed two distinct mass loss events at 50 °C and 360 °C, corresponding to the desorption of physisorbed volatiles (*e.g.*, water and residual reactants) and the combustion of soft coke deposits, respectively.[42] PXRD analysis showed no evidence of metal aggregation or hard coke formation, confirming that structural integrity was maintained during operation. Taken together, the results from TGA, XRD, and reactivity testing point to soft coke deposition as the primary, and fully reversible, deactivation mechanism under the conditions examined.

PMCL synthesis, recyclability, and properties

To validate the quality of the monomer MCL obtained by our current synthetic method, the MCL generated by the hereindescribed synthetic route was used for polymerization without further purification steps, except for simple degassing and drying by storage over molecular sieves (^1H NMR shown in Fig. S12). Azobisisobutyronitrile (AIBN) was used as a radical initiator and the polymerization was performed at 80 °C over 24 h in 2 M toluene solution, resulting in 43% conversion of MCL to PMCL (Fig. S13). SEC of the isolated PMCL yielded a number-average molecular weight M_n = 62.5 kDa and dispersity $Đ$ = 1.86 (Fig. S14). Differential scanning calorimetry (DSC) revealed that PMCL exhibits a T_g of 168 °C (Fig. S15), which is considerably higher than PMMA (~110 °C), but lower than analogous PMVL, an expected result due to the plasticizing effects of the methyl group in the δ-position of MCL.[5] The decomposition temperature ($T_{d5\%}$, defined as the temperature at 5% mass loss) was determined with TGA as 298 °C (Fig. S16). The optical clarity of the material was comparable to PMMA, determined by high transmittance of the sample (89%) in the visible light wavelength range (Fig. S17).[43,44] Next, we examined the polymerization of MCL *via* coordination-addition polymerization using tris(benzyloxy)lanthanum {[La$(OBn)_3]_x$} as the catalyst and initiator, which is expected to be highly reactive due to the conjugated MCL structure and locked s-*cis* conformation.[5,45] Over 6 h, the reaction reached 99% monomer conversion to PMCL (Fig. S18), and the isolated PMCL showed a high molecular weight (M_n = 470 kDa, $Đ$ =

1.46) (Fig. S19), along with similar thermal properties to the radically initiated polymer (Fig. S20 and S21). Together, these results showed that our synthetic method is successful in producing polymerization-grade MCL, which can be readily polymerized through different mechanisms without requiring additional purification steps.

As a comparison, we applied the same radical polymerization conditions to the independently synthesized MCL (Fig. S22), which was prepared through a standard method, analogous to those previously reported for MVL and MDL.[5] Notably, this monomer achieved almost identical conversion (44%) to PMCL as the initial run (Fig. S23), and the isolated material likewise exhibited a similar molecular weight with M_n = 65.5 kDa ($Đ$ = 1.96) (Fig. S24) and thermal properties (Fig. S25 and S26). These results further confirmed that the MCL synthesized by the new method reported in this work has the same quality and polymerizability as the one obtained by the standard organic synthesis.

After demonstrating the polymerizability of the MCL obtained by the new method, we sought to investigate the chemical recyclability of PMCL back to its virgin-quality monomer. We reasoned that we could apply the established depolymerization conditions for PMVL to PMCL due to their structural similarity.[5] Hence, we subjected PMCL to a reactive distillation setup at 220 °C under 50 mTorr over 11 h, successfully recovering the reformed MCL in 74% isolated yield and in high purity (Fig. S27), along with 12% remaining non-volatile PMCL oligomers (Fig. S28), which could be reused for the next depolymerization to recover more monomer. It is important to note that this depolymerization temperature is only possible under non-equilibrium conditions, wherein monomer is continuously removed from the system to drive the reaction to completion. It is, therefore, not a representative degradation temperature under standard conditions. These results demonstrate the markedly improved recyclability of PMCL relative to PMMA, the latter of which requires significantly higher temperatures for appreciable monomer recovery under bulk depolymerization conditions.[45]

Conclusions

We present a catalytic approach to produce PMCL from TAL through sequential hydrogenation and dehydration of TAL to dCL, aldol condensation to MCL, and vinyl addition polymerization to PMCL. TAL hydrogenation was evaluated over supported Pd, Pt, and Ru on various supports, with 5 wt% Ru/C achieving 98% HMTHP yield at complete conversion under 35 bar H_2 at 60 °C. For the subsequent conversion of HMTHP to dCL, Pt catalysts supported on Al_2O_3, SiO_2, TiO_2, and CeO_2 were studied to facilitate C–O bond cleavage. From these, a 1 wt% Pt/TiO_2 resulted in the highest dCL yield (88%) at complete HMTHP conversion under 35 bar H_2 at 160 °C. Aldol condensation of dCL with formaldehyde over Cs_2O/SiO_2 produced up to 92% MCL yield under optimized conditions. Polymerization of MCL produced PMCL with enhanced heat resistance (higher T_g) and chemical recyclability (higher monomer recovery yield under lower reaction temperature), as compared to PMMA. This study presents a viable route to more sustainable PMMA alternatives using catalysis and bio-based feedstock and intermediates.

Conflicts of interest

There are no conflicts to declare.

Data availability

The data supporting this study are available in figures and tables within the article and in the supplementary information (SI). Supplementary information contains catalyst characterization data (BET, CO chemisorption, CO_2 uptake, XRD, HAADF-STEM, STEM-EDS); ^{1}H, ^{13}C, and HSQC NMR spectra of HMTHP, MCL, and PMCL; GC chromatograms and additional aldol condensation reactivity and catalyst stability data; and SEC, DSC, TGA, and UV-vis transmittance data for the PMCL samples. See DOI: https://doi.org/10.1039/d6gc01148a.

Acknowledgements

Funding was provided by the U.S. Department of Energy Office of Critical Minerals and Energy Innovation from the Advanced Materials and Manufacturing Technologies Office (AMMTO) and the Alternative Fuels and Feedstocks Office (AFFO). This work was performed as part of the Bio-Optimized Technologies to keep Thermoplastics out of Landfills and the Environment (BOTTLE) Consortium and was supported by AMMTO and AFFO under Contract DE-AC36-08GO28308 with the National Laboratory of the Rockies (NLR). The BOTTLE Consortium include members from the University of Puerto Rico-Mayaguez, Massachusetts Institute of Technology and Colorado State University, funded under contract DE-AC36-08GO28308 with NLR. The work on de/polymerization was also supported by RePLACE (Redesigning Polymers to Leverage A Circular Economy) funded by the Office of Science of the U.S. Department of Energy *via* award # DE-SC0022290. STEM analysis was carried out in part through the use of MIT.nano's facilities. Optical properties of PMCL were determined using instrumentation available through the Colorado Shared Instrumentation in Nanofabrication and Characterization (COSINC). The views expressed in the article do not necessarily represent the views of the DOE or the U.S. Government.

References

1 L. O. Mark, M. C. Cendejas and I. Hermans, *ChemSusChem*, 2020, **13**, 5808–5836.
2 A. A. Khechfe, F. D. Eckstrom, E. R. Chokkapu, L. A. Baston, B. Liu, E. Y. X. Chen and Y. Román-Leshkov, *Green Chem.*, 2024, **26**, 10463–10472.

3 Z.-H. Zhang, X. Wang, B. Weng, Y. Zhang, G. Zhang and M. Hong, *ACS Polym. Au*, 2022, **2**, 266–274.
4 D. Kiani, R. Eaglesfield, J. H. May, A. Z. Werner, E. Y. X. Chen, Y. Román-Leshkov, Y. J. Pagán-Torres and G. T. Beckham, *Nat. Rev. Chem.*, 2025, **9**, 749–765.
5 R. A. Gilsdorf, E. R. Chokkapu, A. Athaley, T. Uekert, R. R. Gowda, A. Singh, J. S. DesVeaux, G. T. Beckham and E. Y. X. Chen, *Cell Rep. Phys. Sci.*, 2024, **5**, 101938.
6 M. M. Demir, M. Memesa, P. Castignolles and G. Wegner, *Macromol. Rapid Commun.*, 2006, **27**, 763–770.
7 A. C. Henry, T. J. Tutt, M. Galloway, Y. Y. Davidson, C. S. McWhorter, S. A. Soper and R. L. McCarley, *Anal. Chem.*, 2000, **72**, 5331–5337.
8 J. J. Shah, J. Geist, L. E. Locascio, M. Gaitan, M. V. Rao and W. N. Vreeland, *Electrophoresis*, 2006, **27**, 3788–3796.
9 G. I. Edo, W. Ndudi, A. B. M. Ali, E. Yousif, K. Zainulabdeen, P. N. Onyibe, P. O. Akpoghelie, H. A. Ekokotu, E. F. Isoje, U. A. Igbuku, A. E. A. Essaghah, D. S. Ahmed and H. Umar, *J. Mater. Sci.*, 2024, **59**, 20496–20539.
10 M. Sponchioni and S. Altinok, *J. Adv. Chem. Eng.*, 2022, **60**, 269–287.
11 N. Silva de Souza Lima Cano, M. U. Hossain and M. M. Bilec, *Waste Manage. Res.*, 2025, **43**, 241–253.
12 S. R. Nicholson, N. A. Rorrer, A. C. Carpenter and G. T. Beckham, *Joule*, 2021, **5**, 673–686.
13 E. Esmizadeh, S. Khalili, A. Vahidifar, G. Naderi and C. Dubois, *Handbook of Ecomaterials*, Springer, 2018, pp. 1–33.
14 Y. Zhuang, N. Saadatkhah, T. D. Nguyen, J. De Tommaso, C. Y. J. Ng, C. Wang, A. Ajji and G. S. Patience, *React. Chem. Eng.*, 2024, **10**, 237–250.
15 O. Guselnikova, O. Semyonov, E. Sviridova, R. Gulyaev, A. Gorbunova, D. Kogolev, A. Trelin, Y. Yamauchi, R. Boukherroub and P. Postnikov, *Chem. Soc. Rev.*, 2023, **52**, 4755–4832.
16 M. Gabrič, F. M. Harth, B. Hočevar, S. Gyergyek, B. Likozar and M. Grilc, *Green Chem.*, 2025, **27**, 3640–3645.
17 H. Fouilloux and C. M. Thomas, *Macromol. Rapid. Commun.*, 2021, **42**, e2000530.
18 A. Bohre, K. Avasthi, U. Novak and B. Likozar, *ACS Sustainable Chem. Eng.*, 2021, **9**, 2902–2911.
19 A. Bohre, U. Novak, M. Grilc and B. Likozar, *Mol. Catal.*, 2019, **476**, 110520.
20 M. J. D. Mahboub, J. L. Dubois, F. Cavani, M. Rostamizadeh and G. S. Patience, *Chem. Soc. Rev.*, 2018, **47**, 7703–7738.
21 Z. Vobecka, C. Wei, K. Tauer and D. Esposito, *Polymer*, 2015, **74**, 262–271.
22 C. M. Wen, C. Foster, W. van Winden and M. Ierapetritou, *ACS Sustainable Chem. Eng.*, 2024, **12**, 12430–12445.
23 K. A. Markham, C. M. Palmer, M. Chwatko, J. M. Wagner, C. Murray, S. Vazquez, A. Swaminathan, I. Chakravarty, N. A. Lynd and H. S. Alper, *Proc. Natl. Acad. Sci. U. S. A.*, 2018, **115**, 2096–2101.
24 D. Xie, Z. Shao, J. Achkar, W. Zha, J. W. Frost and H. Zhao, *Biotechnol. Bioeng.*, 2006, **93**, 727–736.
25 W. Zha, Z. Shao, J. W. Frost and H. Zhao, *J. Am. Chem. Soc.*, 2004, **126**, 4534–4535.
26 M. S. Kim, L. Shi, H. Zhao and G. W. Huber, *ACS Sustainable Chem. Eng.*, 2025, **13**, 2380–2387.
27 S. S. Bhagwat, M. N. Dell'Anna, Y. Li, M. Cao, E. C. Brace, S. S. Bhagwat, G. W. Huber, H. Zhao and J. S. Guest, *ACS Sustainable Chem. Eng.*, 2025, **13**, 17794–17805.
28 M. S. Kim, D. Choi, J. Ha, K. Choi, J. H. Yu, J. A. Dumesic and G. W. Huber, *ACS Catal.*, 2023, **13**, 14031–14041.
29 M. S. Kim, S. S. Bhagwat, L. Santiago-Martínez, X. Shi, K. Choi, J. S. Guest and G. W. Huber, *Green Chem.*, 2025, **27**, 6087–6104.
30 J. Demarteau, B. Cousineau, Z. Wang, B. Bose, S. Cheong, G. Lan, N. R. Baral, S. J. Teat, C. D. Scown, J. D. Keasling and B. A. Helms, *Nat. Sustain.*, 2023, **6**, 1426–1435.
31 M. Chia, T. J. Schwartz, B. H. Shanks and J. A. Dumesic, *Green Chem.*, 2012, **14**, 1850–1853.
32 M. Chia, M. A. Haider, G. Pollock, G. A. Kraus, M. Neurock and J. A. Dumesic, *J. Am. Chem. Soc.*, 2013, **135**, 5699–5708.
33 S. A. D'Ippolito, C. Especel, L. Vivier, F. Epron and C. L. Pieck, *Appl. Catal., A*, 2014, **469**, 532–540.
34 S. A. Tacey and C. A. Farberow, *J. Phys. Chem. C*, 2025, **129**, 7238–7247.
35 X. Zhao, X. Wu, H. Wang, J. Han, Q. Ge and X. Zhu, *ChemistrySelect*, 2018, **3**, 10364–10370.
36 A. Miró i Rovira, J. Skjæveland, K. Rajendran, T. Bergh, P. Tingelstad, R. Myrstad and D. Chen, *Top. Catal.*, 2025, **68**, 2549–2564.
37 R. Shu, B. Lin, C. Wang, J. Zhang, Z. Cheng and Y. Chen, *Fuel*, 2019, **239**, 1083–1090.
38 L. E. Manzer, *Appl. Catal., A*, 2004, **272**, 249–256.
39 M. Al-Naji, B. Puértolas, B. Kumru, D. Cruz, M. Bäumel, B. V. K. J. Schmidt, N. V. Tarakina and J. Pérez-Ramírez, *ChemSusChem*, 2019, **12**, 2628–2636.
40 J. Tai and R. J. Davis, *Catal. Today*, 2007, **123**, 42–49.
41 Q. Bao, T. Bu, J. Yan, C. Zhang, C. Ning, Y. Zhang, M. Hao, W. Zhang and Z. Wang, *Catal. Lett.*, 2017, **147**, 1540–1550.
42 H. Zhang, S. Shao, R. Xiao, D. Shen and J. Zeng, *Energy Fuels*, 2014, **28**, 52–57.
43 Z. K. Heiba, M. B. Mohamed and N. G. Imam, *J. Inorg. Organomet. Polym. Mater.*, 2016, **26**, 780–787.
44 A. Tilioua, *Mater. Sci. Energy Technol.*, 2021, **4**, 349–356.
45 R. A. Gilsdorf, M. A. Nicki and E. Y. X. Chen, *Polym. Chem.*, 2020, **11**, 4942–4950.

